Imaging tropical peatlands in Indonesia using ground penetrating radar (GPR) and electrical resistivity imaging (ERI): implications for carbon stock estimates and peat soil characterization.

Xavier Comas *[1], Neil Terry [2], Lee Slater [2], Matthew Warren [3], Randy Kolka [4], Agus Kristijono [5], Nana Sudiana [5], Dadan Nurjaman [5], Taryono Darusman [6].

[1] Department of Geosciences, Florida Atlantic University, Davie, FL 33314 USA

[2] Department of Earth & Environmental Sciences, Rutgers-Newark, Newark, NJ 07102 USA

[3] USDA Forest Service, Northern Research Station, Durham NH 03824 USA

[4] USDA Forest Service, Northern Research Station, Grand Rapids MN 55744 USA

[5] Indonesian Agency for Assessment and Application of Technology (BPPT), Jakarta 10340 Indonesia

[6] United States Forest Service affiliate, Puter Foundation

Abstract

Current estimates of carbon (C) storage in peatland systems worldwide indicate tropical peatlands comprise about 15% of the global peat carbon pool. Such estimates are uncertain due to data gaps regarding organic peat soil thickness, volume and C content. We combined a set of indirect geophysical methods (ground penetrating radar, GPR, and electrical resistivity imaging, ERI) with direct observations using core sampling and C analysis to determine how geophysical imaging may enhance traditional coring methods for estimating peat thickness and C storage in a tropical peatland system in W. Kalimantan, Indonesia. Both GPR and ERI methods demonstrated capability to estimate peat thickness in tropical peat soils at a spatial resolution not feasible with

25 traditional coring methods. GPR is able to capture peat thickness variability at centimeter scale
26 vertical resolution, although peat thickness determination was difficult for peat columns
27 exceeding 5 m in the areas studied, due to signal attenuation associated with thick clay-rich
28 transitional horizons at the peat-mineral soil interface. ERI methods were more successful for
29 imaging deeper peatlands with thick organomineral layers between peat and underlying mineral
30 soil. Results obtained using GPR methods indicate less than 3% variation in peat thickness
31 (when compared to coring methods) over low peat-mineral soil interface gradients (i.e. below
32 0.02 deg) and show a substantial impacts in C storage estimates (i.e. up to 37 MgC/ha even for
33 transects showing a difference between GPR and coring estimates of 0.07 m in average peat
34 thickness). The geophysical data also provide information on peat matrix attributes such as
35 thickness of organomineral horizons between peat and underlying substrate, the presence of
36 buried wood, buttressed trees or tip-up pools and soil type. The use of GPR and ERI methods to
37 image peat profiles at high resolution can be used to further constrain quantification of peat C
38 pools and inform responsible peatland management in Indonesia and elsewhere in the tropics.
39

40 **1. Introduction**

41 Globally, tropical peatlands are estimated to store 89 PgC, equivalent to about one-tenth
42 of the current atmospheric carbon pool (Page et al. 2011). Indonesia contains the largest area of
43 the world's tropical peatlands, with estimates ranging from 14.9 Mha (Ritung et al. 2011) to
44 21Mha ((Wahyunto et al. 2003, 2004, Page et al. 2011). Indonesian peat swamps have been
45 globally significant carbon sinks over the past 15,000 years (Dommain et al. 2014), however vast
46 areas of Indonesian peatlands are becoming large, long-term sources of greenhouse gases
47 (primarily CO_2) to the atmosphere due to deforestation, drainage and/or peat fires (Page et al.
48 2002, van der Werf et al. 2009). In a recent overview of carbon distribution based on a 2008

49 inventory, Indonesia was considered the largest source of CO_2 emissions from degrading peat
50 worldwide, with values exceeding other large producers such as China and the United States by
51 almost one order of magnitude (Joosten 2009). Therefore, Indonesia's peatlands are considered
52 "hot spots" for greenhouse gas emissions, and are priority areas for climate mitigation strategies
53 including programs such as Reducing Emissions from Deforestation and Forest Degradation (or
54 REDD+). However, data deficiencies regarding area, depth, volume and carbon density of
55 Indonesian peatlands contribute to large uncertainties in carbon pools and fluxes at local to
56 national scales. Such lack of information may also contribute to management decisions which
57 exacerbate greenhouse emissions from peatland degradation. Refinement of estimates on depth
58 and volume of peat soils in Indonesia is the focus of this paper.
59 Current estimates of C storage in global peatlands range between 528-694 Pg C (Hooijer
60 et al. 2006, Yu et al. 2010). Tropical and subtropical systems are estimated to comprise about
61 15% of the global peat carbon pool, with Indonesia estimated to contain about 65% of tropical
62 peat carbon (Page et al. 2011). However, these estimates are tentative due to uncertainties in peat
63 thickness, volume and C density at large spatial scales. Estimating peat carbon storage requires
64 accurate volume measurements calculated from peat area and thickness. Page et al. (2011)
65 calculated peat volume for Indonesia using a mean peat depth of 5.5 m, which was based on very
66 few geographically biased data considering the scale at which the mean depth estimate was
67 applied: 206,950 km^2 throughout Indonesian Borneo (Kalimantan), Sumatra and Papua. Perhaps
68 the most accurate peat volume measurements published at a local scale in Indonesia were
69 reported by Jaenicke et al. (2008) who modeled peat depth using a combination of 542 discrete
70 field measurements from direct coring, surface elevation models, satellite imagery and spatial
71 interpolation across four peat domes in Central Kalimantan. Despite the large number of direct
72 measurements of peat thickness, the uncertainty in carbon storage estimates ranged from 13-

25%, which the authors attributed to bedrock unconformities not considered in the models of peat volume derived from relationships between surface elevation and peat thickness (Jaenicke et al. 2008). Most current efforts to model peat depth are based on the assumption that peat deposits occur in uniform biconvex formations, despite evidence from field measurements indicating considerable buried topography under the peat in some areas such as riverbeds and levees. For example, surveys have shown mineral substrate topography changing as much as 2 m within single transects (of less than one km) across several peat domes in Borneo (Konsultant 1998, Dommain et al. 2010).

Near surface geophysical methods, particularly ground penetrating radar (GPR), have been used extensively in boreal peatland systems to explore many aspects related to peat development and stratigraphy (Comas and Slater 2009). Recent studies of peat thickness and peat basin volume using GPR include a variety of field sites and typically indicate discrepancies in peat volume estimates of about 20% when compared to traditional direct methods such as coring (Rosa et al. 2009, Parsekian et al. 2012, Parry et al. 2014). Electrical resistivity imaging (ERI) has also been used in boreal systems for investigating several aspects of peatland stratigraphy and hydrogeology (Meyer 1989, Slater and Reeve 2002, Comas et al. 2004, Comas et al. 2011), however no studies to our knowledge have focused on peat thickness characterization using ERI. Although numerous studies have used GPR and ERI methodologies to study peatland attributes in boreal systems, the use of these techniques in tropical systems has not been reported. Although differences in peat types, terrain and/or vegetation cover between boreal and tropical systems must be considered, similarities in peat electromagnetic and electrical properties are anticipated, supporting the use of GPR and ERI methods for mapping tropical peatlands and underlying buried topography.

Here we report the use of a combination of GPR and ERI methods to obtain high resolution profiles of peat layers in West Kalimantan, Indonesia. The objectives of this study were to 1) test the potential of GPR and ERI for estimating peat thickness in a non-invasive and spatially continuous way at a resolution previously unreported for tropical peatlands; and 2) evaluate whether certain information on geological settings and/or peat composition can be drawn from these methods. The ultimate aim of the approach presented here is to demonstrate the applicability of geophysical methods to investigate tropical peat systems, and to highlight potential for improved accuracy of peat C storage estimates relative to estimates derived from traditional coring methods. Advancing this knowledge could inform peatland management decisions in Indonesia and improve assessments of peat subsidence and C stock changes.

2. Methods

2.1 Field Sites

Two peatland sites located in the West Kalimantan Province were chosen for this study: Tanjung Gunung (Sejahtera village, Kayong Utara District); and Pelang (Pelang village, Ketapang District). Both sites had been previously investigated by USFS (United States Forest Service) collaborators and were known to contain variable peat thickness and multiple landcover types, while providing relatively easy access. The Tanjung Gunung site (hereafter referred to as TG) is adjacent to Gunung Palung National Park and its natural resources have been heavily exploited by the local community for decades. Within the TG site, two areas along the same peat formation were studied: a thinned, degraded forest (TG1) and a mature rubber plantation which is located at the edge of the peat formation (TG2). The physiographic terrain at TG is a 6 km wide swamp peatland known as Mendawai, MDW (RePPProT, Regional Physical Planning Programme for Transmigration, (1990) that is characterized by shallow peat. Kahayan (KHY)

peaty alluvial plains are also formed along the seaward edges of MDW (inset in Figure 1). Although the two selected study sites (TG1 and TG2) are only approximately 1 km apart and are both situated in a transition zone between KHY and MDW ecosystems, differences exist in terms of thickness of peat and organomineral transitional layers and water table depth. While TG1 is characterized by MDW properties (i.e. shallow peat swamps), TG2 is characterized by a mixture of MDW and KHY properties, including landforms such as coalescent estuarine and riverine plains with lithologies that include alluvium and marine sediments.

At the Pelang forest site (hereafter referred to as P), two areas along the same peat formation were also studied: a thinned, degraded forest occurring on approximately 4-5m deep peat (P1), which transitioned to a cleared area covered in secondary ferns and grasses, and a degraded forest (P2) heavily used by a local village occurring on very deep peat (>9m). Compared to the Tanjung Gunung sites (TG1 and TG2), Pelang Forest sites are characterized by extensive peatlands over about 20 km x 20 km (inset in Figure1), forming three types of peat ecosystems: a) Klaru (KLR) or permanently water logged peaty floodplains; b) Gambut (GBT) or deeper dome-shaped peat swamp; and c) Mendawai (MDW) or shallower peat swamp. Similar to the previous sites at TG, Kahayan (KHY) peaty alluvial plains are also formed along the seaward edges of MDW (Figure 1). Two measurement sites were also selected at this location and included P1 (located at a boundary zone of GBT and MDW), whereas site P2 is located within GBT. The results of 2D resistivity measurements described below show significant differences in these two ecosystems. Additional specifications for each study site are summarized in Table 1, including a description of the landcover, average peat depth and land system after RePPProT (1990).

2.2 Ground Penetrating Radar

144 Ground penetrating radar (GPR) is a fast, reliable, and inexpensive geophysical method
145 for non-destructive mapping of shallow subsurface features in peatlands at scales ranging from
146 kilometers for geological features influencing peatland hydrology such as eskers (Comas et al.
147 2011), to centimeters for determination of bubble distribution in peat blocks at the laboratory
148 scale (Comas and Slater 2007). The GPR technique involves the transmission of short pulses of
149 high frequency electromagnetic (EM) energy into the ground, and measurement of the energy
150 reflected from interfaces between subsurface materials with contrasting electrical properties. In
151 the most common deployment, one antenna (the transmitter) radiates short pulses of EM waves,
152 and the other antenna (the receiver) measures the reflected signal as a function of time.
153 Reflections are primarily caused by changes in water content, which in turn are determined by
154 sediment type and soil density. Reliable estimates of EM wave velocity (v), primarily controlled
155 by relative dielectric permittivity $\varepsilon_{r(b)}$, are required to convert the EM wave travel times recorded
156 by GPR to depths of significant reflectors. Due to the high water content of peat soils, $\varepsilon_{r(b)}$ of
157 peat is very high compared to inorganic mineral soils, being reaching values of 50-70 depending
158 on peat type. When $\varepsilon_{r(b)}$ is generally well constrained from velocity analysis, estimation of peat
159 depth is typically accurate to within ~20 cm (Parsekian et al. 2012).
160 GPR surveys were performed using a Mala-RAMAC system with 50, 100, and 200 MHz
161 antennas, with the 100 MHz antennas proving the best compromise between depth of
162 investigation and resolution. Malfunctioning of the 50 MHz antennas towards the end of the
163 campaign prevented testing depth of penetration for this frequency at study sites with thicker
164 peat columns. The spacing between traces was 0.2 m and 16 stacks (or replicates) were used for
165 each trace. Two types of surface GPR surveys were performed: 1) common offset surveys, where
166 both transmitter and receiver antennas are kept at a constant distance as they are moved along
167 transects; and 2) common mid-point (CMP) measurements where transmitter and receiver are

168 separated incrementally to larger distances. Common offset surveys were used for subsurface
169 imaging purposes (since profiles resemble a geological cross-section where depth is expressed as
170 a travel time of the EM wave), whereas CMPs were used for velocity estimation.
171
172 **2.3 Electrical Resistivity Imaging**
173 ERI is a method for generating images of the variation in electrical resistivity in either 2
174 or 3 dimensions below a line or grid of electrodes placed at the earth's surface. Data are acquired
175 by measuring the voltage differences between electrode pairs in response to current injection
176 between additional electrode pairs. Numerical methods are used to solve the Poisson equation
177 relating the theoretical voltages at the electrodes to the distribution of resistivity in the
178 subsurface. Inverse methods are used to find a model for the subsurface resistivity structure that
179 is consistent with the recorded field data and also conforming to model constraints imposed
180 (typically the resistivity structure varies smoothly). The resulting resistivity structure describes
181 variations in the ability of subsurface soils and rocks to conduct an electrical current. The
182 resistivity is strongly controlled by water content, chemical composition of the pore water and
183 soil surface area/grain particle size distribution.
184 Electrical resistivity imaging was conducted using a four electrode Wenner configuration
185 with both 1 m and 2 m electrode spacing and providing maximum imaged depths of about 16 m.
186 The imaging depth was estimated from the model resolution matrix (Menke 1989)); see Binley
187 and Kemna (2005) for further details) that depicted relatively good resolution within this region
188 when compared with the rest of the modeling domain. Measurements were performed using an
189 ARES (Automatic Resistivity System) G4 2A resistivity meter with a 48 multi-electrode switch
190 box. Inversion and forward simulations were performed with R2 software written by Andrew
191 Binley (Lancaster University). R2 uses an iterative finite element method to estimate resistivity

values at user-specified element locations in a finite element mesh. The regularization was based on the popular smoothness constrained approach used to solve for the minimum structure resistivity model that satisfies the data constraints.

A triangular mesh with length one quarter of the spacing at the electrodes and growing larger toward the edges (to account for decaying model resolution) was built using Gmsh, a three-dimensional finite element mesh program (Geuzaine and Remacle 2009). R2 requires an estimate of the error associated with each data point for convergence to be evaluated. For this purpose, it is best practice to collect reciprocal data (a companion dataset where current and potential electrodes are reversed) to gain an informed estimate of the errors associated with ERI measurements (Slater et al., 2000), since underestimating these errors can produce image artifacts in the final ERI result which can mistakenly be interpreted as real structures. In lieu of reciprocal data, we employed a 2% error model as input to R2 given the low electrical noise expected in our remote field sites and stacking errors (recorded on the instrument) of less than 1.1%.

2.4 Coring and C storage estimation

A total of nine core samples were obtained along the linear transects established for geophysical surveys using an Eijkelkamp Russian style peat auger inserted vertically into the peat layer. Representative 5 cm peat soil subsamples were taken at depth intervals 0-30, 30-50, 50-100 cm and each subsequent 100 cm interval until mineral substrate was reached. After extraction of core samples, water tables were directly measured using a measuring tape. The length of the sampling device was 9 m, so detection of any deeper boundaries below 9 m using direct methods was not possible. Peat layers were described in the field as “peat”, “transitional” (a mixing horizon of peat and mineral soil) and “mineral soil” (mostly marine derived fine silt

and clay), which represented underlying mineral substrate. The 5 cm subsamples were oven dried at 60 °C until constant weight was achieved, and weighed for bulk density determination. Peat samples were then sent to the USFS Northern Research Station soil analysis laboratory for carbon analysis. Samples were finely ground, homogenized, and analyzed for total C using a LECO TruSpec elemental CN analyzer (LECO Corp, St. Joseph Michigan). Laboratory standards and analytical duplicates were run every 10 samples to ensure data quality. Peat carbon storage was calculated as:

$$C_{peat} = V*C_d \quad (1)$$

where C_{peat} is carbon storage (MgC ha^{-1}); V is peat volume (m^3), the product of area (ha) and depth (cm); and C_d is peat carbon density (kg C m^{-3}), the product of peat bulk density (kg m^{-3}) and carbon content (%C).

2.5 Geophysical surveys

A set of geophysical surveys combined with direct sampling at each study site consisted of: 1) one or more GPR common offset transects between 30-100 m long to identify the peat-mineral soil reflector and other stratigraphic features (such as presence of layers rich in woody debris or buried buttressed trees) within the peat soil reflection record; 2) one or more GPR common mid-point surveys to estimate EM wave velocity along the peat column and convert two-way travel time into depth for common offset profiles; 3) one or more electrical resistivity transects between 48-144 m long to provide additional information related to: a) peat thickness in regions where GPR was anticipated to fail due to thicknesses being greater than the GPR penetration depth and/or excessive GPR attenuation associated with high electrical conductivity; and b) variations in the lithology of the sub-peat mineral deposits; and 4) one or more direct soil cores in order to confirm depth of the peat-mineral soil interface and to obtain samples for subsequent C analysis

240 at selected locations. Since not every core collected was analyzed for C content, Table 2 presents
241 a summary of cores collected including average C percent and content along the peat column.
242
243 **3. Results**
244 **3.1 Tanjung Gunung: shallow peat (0-4 m)**
245 A set of two orthogonal common-offset profiles were collected at Site TG1 with the 0 m
246 distance in Line 1 (Figure 2a) crossing Line 2 (Figure 2b) at 24 m along the profile. An average
247 EM wave velocity of 0.04 m ns^{-1} for the peat column was estimated from GPR common mid-
248 point profiles (not shown here for brevity). Using this velocity estimate, GPR common offset
249 profiles (Figure 2) identified a 4 m thick peat column that is laterally continuous over the profile.
250 Direct coring at two locations (shown in Figure 2a and 2b respectively) confirms a total peat
251 thickness of 4 m with a 0.1-0.2 m sandy clay transition (also containing some organics) into a
252 clayey mineral soil at about 4.2 m depth. Direct coring also detected the presence of: 1) a water
253 table at 0.5 m depth coinciding with the presence of a distinctive reflector in the GPR record
254 (particularly clear in Figure 2b); 2) a woody area between 2-3 m depth (indicated in Figure 2)
255 resulting in isolated points of core refusal that coincide with the presence of hyperbolic
256 diffractions in the reflection record. Extracted core samples showed an average of 58.5 % C and
257 C content of 2,311.0 Mg ha^{-1} (Table 2).
258 Electrical resistivity imaging results for Line 1 and Line 2 at Site TG1 are shown in
259 Figure 3a and 3b respectively. Direct cores as shown in Figure 2 are superimposed for
260 comparison. The resistivity inversion shows a relatively conductive (resistivity less than 100
261 Ohm m) upper layer, underlain by a more resistive unit of undetermined thickness. The upper
262 layer (showing a progressive increase in resistivity with depth between 60-200 Ohm m)
263 correlates with the terrestrial peat deposit as confirmed from direct sampling and GPR. The

underlying resistive layer (ranging between 200-300 Ohm m) includes both a transition layer composed of a mixture of sand and clay (with some organics) and a clayey mineral soil as confirmed from coring. Although lower resistivities are typical for clayey mineral sediments that are usually found below peat, in this case the higher resistivities are attributed to a sandy mineral soil matrix as confirmed from coring in the transition layer.

GPR common offset profiles at Site TG2 (Figure 4 and 5) identified a variable peat column ranging between 0.1-3.4 m along the profiles. An average EM wave velocity of 0.038 m ns^{-1} for the peat column (slightly lower than that at TG1) was estimated from GPR common mid-point profiles. As shown in the reflection record in Figure 4a and confirmed with direct coring, the reflector interpreted as the peat-mineral soil interface deepens from the surface (at 70 m along the profile where the reflector is not discernible from the ground coupling) to 1.5 m (at 74 m along the profile) towards the NE, representing a total increase of 1.4 m in peat thickness over a 4 m horizontal distance (i.e. between 70 and 74 m along the profile). This trend extends to the end of the profile where the peat-mineral soil exceeds depths of 3 m, where peat thickness increases by over 3 m in about 20 m along the transect. The ERI images are consistent with this interpretation (Figure 4b) depicting a resistive upper layer (100-370 Ohm m interpreted as peat) underlain by a conductive unit (as low as 20 Ohm m) interpreted as clay and confirmed from both coring and surface outcrops between 0 and 60 m along the transect. Figure 5a represents the continuation of the GPR common offset profile in Figure 4a towards the NE. In this case peat thickness is almost uniform (as confirmed with coring and depicted in Figure 5a), with peat thickness changing only by 0.4 m across the 100 m long profile. This profile also confirms the presence of a distinctive reflector at about 0.8 m depth interpreted as the water table as confirmed from coring. Although the coring did not explicitly detect points of core refusal (like those at TG1), the GPR record also shows the presence of hyperbolic diffractions in the

reflection record (i.e. between 40-85 m along the transect and between 2-3 m depth in Figure 5a as indicated by white arrows). The ERI image in Figure 5b follows the GPR profile in Figure 5a and is consistent with the results shown in Figure 4b depicting a resistive upper layer (100-370 Ohm m interpreted as peat) underlain by a conductive unit (as low as 20 Ohm m) interpreted as clay. For TG1.1-TG1.3, the organic soil had an average C percent of 49.3 % C and C content of 1,683.4 Mg ha^{-1} (Table 2).

3.2 Pelang Forest: intermediate and deep peat (5-9 m)

Geophysical surveys constrained with direct coring at Pelang Forest contrast with those previously described at Tanjung Gunung by showing greater peat thicknesses ranging between 5 m at Site P1 up to 9 m at Site P2. GPR and electrical resistivity surveys at Site P1 were collected at different locations separated by about 1 km since GPR transects at this site were not accessible with heavy resistivity instrumentation. Similar to Site TG1, an average EM wave velocity of 0.04 m ns^{-1} for the peat column was estimated from GPR common mid-point profiles at this site. GPR common offset profiles at Site P1 (Figure 6) show a reflection record characterized by: 1) a depth of penetration of 5 m followed by signal attenuation that coincides with a sandy clay transition (with some organics) between 5-7.5 m underlain by a clayey mineral soil as confirmed from coring (shown at 95 m along the profile in Figure 6); 2) a distinct reflector at about 35-40 ns interpreted as the water table; 3) a sequence of laterally discontinuous chaotic reflectors with some hyperbolic diffractions (i.e. as seen at 150 ns and 15 m along the profile and indicated by a small white arrow); and 4) a possible depression feature within the peat column between 150-250 ns and 10-35 m along the profile, with a SE side tilting about 9 degrees towards the NW and a NW side tilting about 13 degrees towards the SE. The white arrow in Figure 6 indicates the lowest point of this feature.

312 Electrical resistivity imaging results at Site P1 (Figure 7) show an interface at about 5 m
313 depth (as confirmed from coring) between an upper resistive layer with a resistivity ranging
314 between 150-300 Ohm m interpreted as peat, underlain by a conductive unit (as low as 30 Ohm
315 m) interpreted as clay and confirmed from coring. These resistivity values are consistent with
316 those previously shown for Site TG2 in Figure 4b. Although boundaries are not clear, a
317 transitional layer along the column between the peat and clay units shows intermediate resistivity
318 values (around 100 Ohm m) and is coincident with the mixture of sand, clay and organics with a
319 thickness of about 2.5 m identified in the coring. Although not directly confirmed from coring, it
320 appears the interface between the peat and the sandy clay is variable across the profile in Figure
321 7, indicating undulating peat thickness between 5 m (i.e. at core location at 22 m along the line,
322 and at 70, 105, or 120 m along the line based on ERI alone) and 7.5-8 m (i.e. at 12, 90, or 130 m
323 along the profile). The ERI profile also shows a strong lateral resistivity variation in the deeper
324 mineral soil (i.e. below 10 m depth) varying between 30-100 Ohm m from the SE to the NW
325 direction. Cores P1.1 and P1.2 averaged 50.8 % C with a C content of 2,677.1 Mg ha^{-1} (Table 2).
326 Variability in peat thickness at Site P2 (Figure 8) is similar to that described for Site P1
327 (Figure 7) and is confirmed at three coring locations (at 10, 50 and 100 m along the profile)
328 resulting in total peat thicknesses of 9 m or more , 8.7 and 8.8 m respectively. Since topography
329 can be considered flat at the scale of measurement used in this profile, these results confirm that
330 the interface between the peat and the underlying sandy clay transition is undulating and that
331 resistivity values for the peat (between 100-185 Ohm m) and transitional layer (below 100 Ohm
332 m) are consistent with those shown in Figure 7. The clay layer imaged with the resistivity profile
333 in Figure 7 (and confirmed from coring in that figure) is also visible in Figure 8 just below the
334 transitional layer and at approximate depths between 10-14 m. For cores P2.1 and P2.2 the soils
335 averaged 57.0 % C with a C content of 5,892.3 Mg ha^{-1} (Table 2).

4. Discussion

4.1. Peat thickness

In general, peat thickness estimates using GPR and ERI were consistent across sites although several differences between methodologies are noted. GPR was particularly effective for characterizing peat thickness for shallow peat columns (i.e. TG1 and TG2 in Figures 2 and 5b respectively) and able to quantify depth of the peat-mineral soil interface at centimeter scale resolution both vertically and laterally from a strong reflector that matched closely with coring results. This reflector resembles the peat-mineral soil interface as typically detected with GPR in boreal peatlands in North America and Europe, exemplified in several studies for those higher latitude systems (Warner et al. 1990, Jol and Smith 1995, Slater and Reeve 2002, Parsekian et al. 2012, Comas et al. 2013). However, the GPR method, as used with antenna frequencies available for this study, was limited for imaging deep (i.e. 9 m or more) peat columns (i.e. Sites P1 and P2) in this study. We attribute these limitations to: 1) thicker peat columns that excessively attenuate the GPR signal, and/or 2) attenuation due to the presence of clay-rich transition layers with high electrical conductivities as depicted by the low resistivity values in P1 and P2 (Figures 7 and 8). Attenuation in clay-rich areas was to be expected since it is well known than the effectiveness of GPR in peatlands is compromised when electrical conductivity of peat is high due to high electrical fluid conduction or high percent of clay fractions (Theimer et al. 1994).

Electrical resistivity imaging also proves useful for detecting changes in peat thickness across sites and for estimating the depth of interface between peat and mineral soil. When compared to GPR, electrical resistivity shows similar imaging capabilities for estimating both shallow and deep peat columns in the study areas (due to larger depths of investigation), although resolution (both vertical and lateral) is lower than that of GPR , particularly as depth

360 increases. The boundaries between the resistive top layer corresponding to the peat and the
361 underlying conductive materials corresponding to the clay and transitional layer are not clear and
362 are depicted by a gradual increase in conductivity (i.e. Figure 4b, 7, and 8). These results are
363 consistent with previous studies in northern peatlands which demonstrate that electrical
364 conductivity is not an accurate indicator of peat thickness when peat is underlain by a conductive
365 layer (Slater and Reeve 2002). The results presented here also confirm the same issue when peat
366 is underlain by a resistive material (Figure 3), which is not uncommon in Indonesia. For
367 example, sandy mineral soils below the organic sediments of other peatlands in Central
368 Kalimantan have been reported (Shimada et al. 2001). Despite these limitations, a good
369 correspondence exists between the limit of the uppermost high resistivity values at sites TG2, P1
370 and P2 (depicted in red and orange in Figures 4b, 7, and 8) and the peat layer interface.
371 Although GPR and ERI datasets presented here are limited in terms of areal extent and
372 scale of measurement, our intent was to test and demonstrate the potential of the methods for
373 estimating peat thickness in tropical peatlands at better resolution than traditional methods (i.e.
374 coring). Therefore, geophysical surveys were developed at plot level scales averaging 100 m
375 long profiles with the aim of upscaling measurements in subsequent studies. Furthermore, the
376 ultimate aim of this work is to increase the accuracy of peat C storage estimates by using
377 methods able to quantify peat thickness at high lateral resolution (i.e. reaching cm for GPR)
378 when compared to coring. It is important to consider that GPR or ERI as applied here detects
379 interfaces representing contrasts in physical properties which can be used to obtain highly
380 accurate estimates of peat volume. When combined with sampling of representative peat soils for
381 C density determination, total peat carbon storage estimates can be largely at the site level..
382
383 **4.2. Peat C stocks**

384 The profile from Site TG-2 in Figure 5 can be used to investigate how subtle changes in
385 peat thickness as detected from GPR (representing a maximum gradient below 0.02 deg) may
386 influence overall peat carbon stock estimates. Figure 9 shows a comparison between a) peat
387 thickness estimated from GPR at a total of 539 locations (or every 0.2 m along the profile shown
388 in Figure 5a) and direct coring at 5 locations (or approximately every 20 m along the profile)
389 (Figure 9a); and b) peat thickness estimated from ERI at a total of 190 locations (interface shown
390 in Figure 5b) and direct coring at 5 locations (Figure 9b). GPR estimates in Figure 9a are based
391 on an average velocity of 0.038 m ns^{-1} for the entire peat column as determined from common
392 midpoint surveys at two different locations at TG2 using two different antenna frequencies (i.e.
393 100 and 200 MHz), and the travel time recorded at the 5 coring locations (consistently showing
394 estimates 0.038 ± 0.001m ns^{-1}). The lower peat boundary was selected from the ERI image using
395 the average inverted resistivity value at pixels corresponding to the interface identified from
396 coring (mean = 131 Ohm-m, standard deviation = 17 Ohm-m). Lateral variability in depth to
397 mineral soil at TG2 ranges between 2.9-3.4 from the GPR and 2.4-3.7 m as estimated from the
398 ERI images (Figure 9a and 9b respectively), confirming that substrate topography is highly
399 variable laterally. These results also confirm previous studies showing lateral variability in
400 mineral substrate topography across several peat domes in Borneo (Dommain et al. (2010) after
401 Konsultant (1998)). Furthermore, these results confirm that vertical resolution of peat profiles
402 obtained from ERI is lower than those obtained using GPR, as expected.
403 Error bars in the GPR data (± 0.05 m average in Figure 9a) were calculated from the
404 difference in peat thickness between GPR using this average velocity and that measured from the
405 coring. Error bars in the ERI data (Figure 9b) were computed as the maximum misfit at each
406 horizontal location between (1) the interpolated interface depth taken from coring and (2) the
407 ERI estimated interface depth using the mean resistivity value ± 2 standard deviations. Assuming

408 that lateral variability in peat thickness between cores is non-existent when the same thickness is
409 estimated for contiguous cores (i.e. perfectly horizontal interface), and that thickness increases
410 gradually with distance (i.e. constant gradient) as shown in the shaded areas in Figure 9a, the
411 overall peat surface area for the profile is estimated to be 324 m^2. Thickness estimated from
412 individual GPR traces (every 0.2 m), produces an overall peat surface area of 331 m^2, an increase
413 of 2.1 %. The difference in surface area represents a total increase of 1,171 kg of C along the two
414 dimensional profile if we assume a C content of 1,673.1 Mg C ha^{-1} as averaged for the peat
415 column in Core TG2.1-TG2.3 (Table 2). Due to the limitations in terms of a) vertical resolution,
416 and b) lateral extent of the profile (i.e. low inversion results on the edges of the profiles) a similar
417 approach using ERI peat thickness estimates is more uncertain and therefore is not included here.
418 Variability in peat thickness was only 2.9-3.4 m (estimated from GPR traces) or 0.4-0.5 m over
419 the 100 m TG2 transect. Although the 7 m^2 difference in surface area between GPR and coring
420 measurements represents only 0.07 m in average peat thickness, when scaled per area the
421 difference between GPR and coring estimates is 37 MgC/ha, which illustrates how relatively
422 small differences in depth estimates can impact overall C storage calculations. Since most peat
423 formations in Indonesia occur at much larger spatial scales (i.e. tens of kilometers or more), GPR
424 surveys over broader areas are shown here to be capable of largely reducing uncertainties
425 regarding peat thickness and C storage. Moreover, as peat C density in tropical peat soils
426 becomes better constrained (Rodríguez et al. 2013), local to regional estimates of peat C storage
427 could be improved through the use of GPR methods to accurately determine peat thickness.
428 Considering peat thickness can also change dramatically over short distances depending on
429 geomorphic setting (e.g.. about 1.5 m difference in peat thickness within only 4 m along the Site
430 TG-2 profile in Figure 4), measuring peat thickness at finer spatial resolution would thus
431 significantly improve current C stock estimates.

4.3. Peat formation

The results presented here also demonstrate potential for using GPR and ERI methods to improve the understanding of processes associated with peatland formation. Differences in the GPR reflection record and contrasts in electrical conductivity between the two study sites (TG and P) are interpreted as differences in peat ecosystem type and developmental history between sites. First, there is a sharp difference between the profiles at TG1 and TG2, as the resistivity profile increases with depth at TG1 (i.e. higher resistivity at the bottom of the profile, Figure 3) whereas it decreases at TG2 (i.e. lower resistivity at the bottom of the profile, Figure 3). Second, the interface between peat-mineral soil at TG1 and TG2 is characterized by a set of 2-3 sharp reflectors in the GPR record (i.e. Figure 2, 4, and 5), that is absent at Site P where reflectors are sharply attenuated when reaching depths corresponding to the transition zone between peat and clay. Third, resistivity results do not show marked differences in terms of electrical conductivity between sites along the peat-clay interface, although coring results show a marked increase in thickness of the transition zone (mostly corresponding to mixtures of clay and sand) with averages between 0.1-0.2 m for Sites TG1 and TG2 and averages reaching 2.5 m for Site P1. These differences may be attributed to two related issues: 1) the developmental history of peatland initiation and formation at each specific site; and 2) the differences in site location as related to physiographic type of terrain and the characteristics of peat ecosystems at each site. As shown in Figure 1, sites TG1 and TG2 correspond to MDW or shallow peat swamp ecosystems while sites P1 and P2 are characterized by GBT or large ombrotrophic peat swamp ecosystems. Coastal peat swamps in Kalimantan have been described as the result of peat accumulation developed on marine clay and mangrove deposits of river deltas and coastal plains during the late Holocene (~5,000 cal BP) (Supiandi 1988, Dommain et al. 2011). As sea levels fell around 5,000 cal BP, sandy beach ridges were exposed and directly colonized by peat swamps and mud flats

were covered by mangroves (Cameron et al. 1989, Dommain et al. 2011, Dommain et al. 2014). While sites at TG may be related to peat swamp colonization over sandy ridges (as reflected by the presence of a highly resistive mineral soil at TG1 and/or a thin transitional layer at both TG1 and TG2), sites at P may be characterized by colonization of mud flats and mangrove deposits (as characterized by much thicker organomineral mixing horizons and potential increased electrical conductivity that results in a marked attenuation in the GPR reflection record, i.e. Figure 6). Furthermore, the ERI profiles also show lateral variation in resistivity associated with variability in the topography of the deeper mineral soil and associated with peat thickness (i.e. Figure 5b and 9b). Local depressions can be also identified in Figure 7 (i.e. around 80-100 m distance along the profile) and suggest that peat soil undulates at a fine scale. Similar features can also found in Figure 8 (i.e. between 20-50 m distance along the profile).

4.4 Peat matrix

Finally, the spatial resolution provided by GPR common offset profiles also shows the potential for better understanding the nature and internal structure of the peat matrix. For example, referring to the presence of hyperbolic diffractions in the GPR record, Figures 2a, 2b, and 5 show the presence of several areas with a high density of diffractions. These diffractions are particularly abundant in Figure 2a between 10-20 m distance along the profile and at 2.5-3 m depth, or in Figure 5 between 70-85 m distance along the profile and between 2-3 m depth (white arrows in Figure 5). Diffractions are associated with the presence of objects that may act as isolated reflector points such as cobbles and boulders (Neal 2004). In this case, we associate hyperbolic diffractions in GPR common offsets to the presence of buried woody debris (as further confirmed through coring). Other investigations in northern peatlands have also related GPR diffractions to the presence of wood (Slater and Reeve 2002). Such features are absent at

P1 (Figure 6) where more laterally continuous reflections (i.e. at 3, 4, and 4.5 m depth between 40 to 90 m along the profile) are present. Previous studies in Kalimantan region have also consistently shown layers with large quantities of undecomposed woody fragments heterogeneously distributed within the peat column (Shimada et al. 2001). Furthermore, some of these laterally continuous reflectors generate a depressional feature between 10 to 30 m along the profile of P1 (center point indicated by a white arrow in Figure 6) as depicted by a sharp reflector at depths between 3.5 to almost 6 m that tilts 13 and 9 degrees respectively on the NW and SE sides of the profile. Although not directly confirmed in the field through direct coring, this feature might be related to the presence of buttressed trees which often prompt the formation of hummocks and water ponding upslope (Dommain et al, 2010), or the uprooting of such trees due to wind and the formation of depressional features as the root zone is displaced. Alternatively, these feature may also be associated to the infill process in a tip-up pool. As described by Dommain et al. (2015) for peatlands in Borneo tip-up pools are commonly formed when lightning strikes a tree inducing its fall and generating a discontinuity in the peat deposit and a pool subsequently infilled with younger material. Because horizontal reflectors seem to overlap the tilting reflectors may support the hypothesis that the depression formed suddenly, to be later filled up progressively with younger peat. Although this may represent an isolated feature in our dataset Dommain et al. (2015) have recently demonstrated the importance of such features when describing carbon accumulation rates and how it may complicate paleo-environmental reconstructions.

5. Conclusions

This study demonstrates the feasibility of using GPR and ERI for non-invasive mapping of the subsurface of peatlands in Indonesia, at a spatial resolution previously unreported in

504 tropical peatland systems which are traditionally assessed using coring methods. The results
505 presented highlight the opportunity to use the reflection record from GPR to improve peat
506 thickness estimates while providing information on certain attributes of the peat matrix such as
507 presence of wood layers or buttressed trees, or peat soil origins related to peatland ecosystem
508 type (i.e. mangrove vs. freshwater peat). While in general GPR is able to predict peat thickness
509 with cm resolution some limitations emerged (i.e. signal attenuation) for peat columns exceeding
510 5 m thick. Although the vertical resolution of ERI is more limited, peat thickness determination
511 shows comparable results for either shallow or deep peat columns. A comparison between peat
512 thickness estimates from GPR, ERI and coring showed a variability exceeding 2 % in peat
513 surface area (or 1,191 kg of C assuming C contents of 170 kg C m^{-2} as averaged from core
514 samples), although this was based on a short 100 m two dimensional profile indicating changes
515 in thickness of less than 0.5 m. Such discrepancies may be larger when considering transects
516 with a more variable peat thickness (such as those here showing up to 1.5 m vertical difference
517 over only 4 m in the horizontal). Given the difficulty of capturing such variability with
518 traditional methods (such as coring), estimating total C stocks in Indonesian peatlands at local
519 scales should be revisited using methods such as GPR or electrical resistivity imaging that better
520 account for lateral variability.
521
522 **6. Acknowledgements**
523 This work was supported by the U.S. Agency for International Development (USAID).
524 We are indebted to Kent Elliot (U.S. Forest Service) for all his help with logistics and fieldwork
525 during this study. We are also thankful to Sofyan Kurnianto (CIFOR/Oregon State University)
526 and Ophelia Wang (USAID-IFACS) for their help in the field, and to all the local Indonesians
527 and helpers involved in this research for their support at the study sites. We thank R. Dommain

528 for helpful discussions and revisions in the materials presented in this study. We also thank four
529 anonymous reviewers and the Editor for helpful comments to improve an earlier version of this
530 manuscript.

531

532 **7. References**

533 Binley, A. and A. Kemna. 2005. DC Resistivity and Induced Polarization Methods.*in* Y. Rubin
534 and S. S. Hubbard, editors. Hydrogeophysics. Springer, New York.
535 Cameron, C.C., J.S. Esterle, and A.P. Curtis. 1989. The geology, botany and chemistry of
536 selected peat-forming environments from temperate and tropical latitudes. International
537 Journal of Coal Geology **12**:105-156.
538 Comas, X. and L. Slater. 2007. Evolution of biogenic gasses in peat blocks inferred from non-
539 invasive dielectric permittivity measurements. Water Resources Research **43**:W05424.
540 Comas, X. , L. Slater, and A. Reeve. 2004. Geophysical evidence for peat basin morphology and
541 stratigraphic controls on vegetation observed in a Northern Peatland. Journal of
542 Hydrology **295**:173-184.
543 Comas, X., N. Kettridge, A. Binley, L. Slater, A. Parsekian, A. J. Baird, M. Strack, and J. M.
544 Waddington. 2013. The effect of peat structure on the spatial distribution of biogenic
545 gases within bogs. Hydrological Processes:doi: 10.1002/hyp.10056.
546 Comas, Xavier, Lee Slater, and A. S. Reeve. 2011. Pool patterning in a northern peatland:
547 Geophysical evidence for the role of postglacial landforms. Journal of Hydrology
548 **399**:173-184.
549 Dommain, R., J. Couwenberg, and H. Joosten. 2010. Hydrological self-regulation of domed
550 peatlands in south-east Asia and consequences for conservation and restoration. Mires
551 and Peat **6**.
552 Dommain, R., J. Couwenberg, P. H. Glaser, H. Joosten, I. Nyoman, and N. Suryaputra. 2014.
553 Carbon storage and release in Indonesian peatlands since the last deglaciation.
554 Quarternary Science Reviews **97**:1-32.
555 Dommain, René, Alexander R. Cobb, Hans Joosten, Paul H. Glaser, Amy F. L. Chua, Laure
556 Gandois, Fuu-Ming Kai, Anders Noren, Kamariah A. Salim, N. Salihah H. Su'ut, and
557 Charles F. Harvey. 2015. Forest dynamics and tip-up pools drive pulses of high carbon
558 accumulation rates in a tropical peat dome in Borneo (Southeast Asia). Journal of
559 Geophysical Research: Biogeosciences:2014JG002796.
560 Dommain, René, John Couwenberg, and Hans Joosten. 2011. Development and carbon
561 sequestration of tropical peat domes in south-east Asia: links to post-glacial sea-level
562 changes and Holocene climate variability. Quaternary Science Reviews **30**:999-1010.
563 Geuzaine, C. and J.F. Remacle. 2009. Gmsh: a three-dimensional finite element mesh generator
564 with built-in pre- and post-processing facilities. International Journal for Numerical
565 Methods in Engineering **79**:1309-1331.
566 Hooijer, A., M. Silvius, H. Woesten, and S. Page. 2006. Peat- CO_2: Assessment of CO_2
567 emissions from drained peatlands in SE Asia; Delft Hydraulics report Q3943.
568 Jaenicke, J., J. O. Rieley, C. Mott, P. Kimman, and F. Siegert. 2008. Determination of the
569 amount of carbon stored in Indonesian peatlands. Geoderma **147**:151-158.

570 Jol, H. M. and D. G. Smith. 1995. Ground penetrating radar surveys of peatlands for oilfield
571 pipelines in Canada. Journal of Applied Geophysics **34**:109-123.
572 Joosten, H. 2009. The Global Peatland CO_2 Picture. Ede.
573 Konsultant, PS. 1998. Detailed Design and Construction Supervision of Flood Protection and
574 Drainage Facilities for Balingian RGC Agricultural Development Project, Sibu Division,
575 Sarawak (Inception Report). Kuching.
576 Menke, W. 1989. Geophysical Data Analysis: Discrete Inverse Theory. Academic. Press, Inc.,
577 New York.
578 Meyer, J.H. 1989. Investigation of Holocene organic sediments: a geophysical approach.
579 International Peat Journal **3**:45-57.
580 Neal, A. 2004. Ground-penetrating radar and its use in sedimentology: principles, problems and
581 progress. Earth-Science Reviews **66**:261-330.
582 Page, S. E., J. O. Rieley, and C. J. Banks. 2011. Global and regional importance of the tropical
583 peatland carbon pool. Global Change Biology **17**:798-818.
584 Page, Susan E., Florian Siegert, John O. Rieley, Hans-Dieter V. Boehm, Adi Jaya, and Suwido
585 Limin. 2002. The amount of carbon released from peat and forest fires in Indonesia
586 during 1997. Nature **420**:61-65.
587 Parry, L. E., L. J. West, J. Holden, and P. J. Chapman. 2014. Evaluating approaches for
588 estimating peat depth. Journal of Geophysical Research: Biogeosciences
589 **119**:2013JG002411.
590 Parsekian, A. D., L. Slater, S. D. Sebestyen, R. K. Kolka, D. Ntarlagiannis, J. Nolan, and P.
591 Hanson. 2012. Comparison of uncertainty in peat volume and soil carbon estimated using
592 GPR and probing. Soil Science Society of America Journal **76**:1911-1918.
593 RePPProT. 1990. Regional Physical Planning Programme for Transmigration. The land
594 resources of Indonesia: a national overview. Main report. Ministry of Transmigration and
595 Land Resources Department/Bina Program., Jakarta.
596 Ritung, S., Wahyunto, K. Nugroho, Sukarman, Hikmatullah, Suparto, and C. Tafakresnanto.
597 2011. Peta Lahan Gambut Indonesia Skala 1:250.000 (Indonesian peatland map at the
598 scale 1:250,000) Indonesian Center for Agricultural Land Resources Research and
599 Development, Bogor, Indonesia.
600 Rodríguez, V., F. Gutiérrez, A.G. Green, D. Carbonel, H. Horstmeyer, and C. Schmelzbach.
601 2013. Characterising saging and collapse sinkholes in a mantled karst by means of
602 Ground Pnentrating Radar (GPR). Environmental and Engineering Geoscience **In Press**.
603 Rosa, E., M. Larocque, S. Pellerin, S. Gagné, and B. Fournier. 2009. Determining the number of
604 manual measurements required to improve peat thickness estimations by ground
605 penetrating radar. Earth Surface Processes and Landforms **34**:377-383.
606 Shimada, Sawahiko, Hidenori Takahashi, Akira Haraguchi, and Masami Kaneko. 2001. The
607 carbon content characteristics of tropical peats in Central Kalimantan, Indonesia:
608 Estimating their spatial variability in density. Biogeochemistry **53**:249-267.
609 Slater, L. and A. Reeve. 2002. Understanding peatland hydrology and stratigraphy using
610 integrated electrical geophysics. Geophysics **67**:365-378.
611 Supiandi, S. 1988. Studies on peat in the coastal plains of Sumatra and Borneo. Part I:
612 Physiography and geomorphology of the coastal plains. Southeast Asian Studies **26**:308-
613 335.
614 Theimer, B. D., D. C. Nobes, and B. G. Warner. 1994. A study of the geoelectrical properties of
615 peatlands and their influence on ground-penetrating radar surveying. Geophysical
616 Prospecting **42**:179-209.

van der Werf, G. R., D. C. Morton, R. S. DeFries, L. Giglio, J. T. Randerson, G. J. Collatz, and P. S. Kasibhatla. 2009. Estimates of fire emissions from an active deforestation region in the southern Amazon based on satellite data and biogeochemical modelling.

Wahyunto, S. Ritung, and H. Subagjo. 2003. Peta Luas Sebaran Lahan Gambut danKandungan Karbon di Pulau Sumatera/Maps of Area of Peatland Distribution and Carbon Content in Sumatera, 1990-2002. Wetlands International e Indonesia Programme and Wildlife Habitat Canada (WHC), Bogor.

Wahyunto, S. Ritung, and H. Subagjo. 2004. Peta Sebaran Lahan Gambut, Luas dan Kandungan Karbon di Kalimantan/Map of Peatland Distribution Area and Carbon Content in Kalimantan, 2000-2002. Wetlands International - Indonesia Programme and Wildlife Habitat Canada (WHC), Bogor.

Warner, B. G., D. C. Nobes, and B. D. Theimer. 1990. An application of ground penetrating radar to peat stratigraphy of Ellice Swamp, southwestern Ontario. Canadian Journal of Earth Science **27**:932-938.

Yu, Z. , J. Loisel, D. P. Brosseau, D. W. Beilman, and S. J. Hunt. 2010. Global peatland dynamics since the Last Glacial Maximum. Geophys. Res. Lett **37**:doi:10.1029/ 2010GL043584.

651 **Table 1**: Summary of field sites including landcover, peat depth (from direct core measurements) and
652 land system after RePPProT, Regional Physical Planning Programme for Transmigration..1990.

Study Site	Landcover	Peat depth (m)	Land system	Description
Tanjung Gunung 1 (TG1)	Thinned forest	3.9-4.3	KHY-MDW transition (MDW)	Shallow peat swamps
Tanjung Gunung 2 (TG2)	Rubber plantation	0.3-3.5	KHY-MDW transition (KHY-MDW)	Shallow peat swamps-estuarine/riverine plains
Pelang Forest 1 (P1)	Disturbed forest	4.0-5.0	GBT-MDW boundary	Deep peat swamp-shallow peat swamp
Pelang Forest 2 (P2)	Thinned forest	>9.0	GBT	Deep peat swamp

653

654

655

656 **Table 2**: Summary of cores including coordinates, landcover, peat depth (from direct coring),C stock
657 along the peat profile (in Mg ha^{-1}) and mean % C in the peat layer.

Core	Coordinates (deg)	Landcover	Peat depth (m)	Peat profile C stock (Mg ha^{-1})	Mean peat bulk density (g cm^{-3})	Mean peat C (% C)
TG1.1	Lat: 110.0699 Long: -1.3036	Thinned Forest	4.1	2300.53	0.10	57.74
TG1.2	Lat: 110.0702 Long: -1.3035	Thinned Forest	4.1	2321.39	0.10	59.33
TG2.1	Lat: 110.0631 Long: -1.2986	Rubber plantation	3.0	1662.02	0.11	52.13
TG2.2	Lat: 110.0633 Long: -1.2989	Rubber plantation	3.0	1764.31	0.16	41.60
TG2.3	Lat: 110.0637 Long: -1.2981	Rubber plantation	3.4	1623.72	0.09	54.20
P1.1	Lat: 110.1524 Long: -1.8644	Disturbed Forest	5.0	3039.36	0.13	49.10
P1.2	Lat: 110.1521 Long: -1.8641	Disturbed Forest	4.3	2314.92	0.12	52.46
P2.1	Lat: 110.1272 Long: -1.8999	Thinned Forest	>9.0	5676.67	0.11	57.82
P2.2	Lat: 110.1277 Long: -1.8997	Thinned Forest	8.3	6107.92	0.13	56.12

658

659

660

Figure captions:

Figure 1: Schematic showing the location of the Study Sites West Kalimantan, Indonesia. A total of four sites were investigated: Tanjung Gunung Site 1 (TG1) and Site 2 (TG2), and Pelang Forest Site 1 (P1) and Site 2 (P2). Inset shows details about the land system as classified after RePPProT (1990): Kahayan (KHY) mainly characterized by alluvial plains; and Gambut (GBT), Mendawai (MDW), and Klaru (KLR) characterized by swamps. Color scale indicates elevation above sea level.

Figure 2: GPR common-offset profile using a Mala GPR system with 100 MHz antennae along Line 1 (a) and Line 2 (b). Location of core samples TG1.1 and TG1.2 and inferred units, water table position and presence of wood layers are also shown. Frame highlights the location of a woody area identified along the cores and characterized by the presence of hyperbolic diffractions in the GPR record.

Figure 3: Inverted images of (a) Line 1 and (b) Line 2 resistivity surveys using a four electrode Wenner type array with 1 m electrode spacing. Location of core samples TG1.1 and TG1.2 and inferred units as per Figure 2 are also shown.

Figure 4: (a) GPR common-offset profile using a Mala GPR system with 200 MHz antennae at study Site TG2. Location of two core samples and inferred units are also shown; (b) Inverted image of resistivity survey along the GPR profile in (a) using a four electrode Wenner type array with 1 m electrode spacing.

Figure 5: (a) GPR common-offset profile using a Mala GPR system with 100 MHz antennae at study Site TG2. The profile represents the continuation of the GPR profile shown in Figure 4 (a). Location of core samples TG2.1-TG.2.3 and two additional core samples and inferred units are also shown. White arrows indicated presence of diffraction hyperbolas; (b) Inverted image of resistivity survey along the GPR profile in (a) using a four electrode Wenner type array with 1 m electrode spacing. Interpreted peat-mineral soil interface is also shown.

Figure 6: GPR common-offset profile using a Mala GPR system with 100 MHz antennae at study Site P1. Location of core sample P1.1 and inferred units and water table position are also shown. Larger white arrow indicates the center of a depressional feature within the reflection record centered between 10-35 m along the profile and 3-5 m depth. Smaller white arrow indicates the presence of a diffraction hyperbola.

Figure 7: Inverted image of resistivity survey at Site P1 using a four electrode Wenner type array with 2 m electrode spacing. Note that resistivity profile does not coincide with location of GPR profile shown in Figure 6. Location of core sample P1.2 and inferred units (depicted in Figure 6) are also shown.

Figure 8: Inverted image of resistivity survey at Site P2 using a four electrode Wenner type array with 2 m electrode spacing. Location of core sample P2.1, P2.2 and one additional location and inferred units (depicted in Figure 6) are also shown.

Figure 9: Comparison of peat thickness estimated from the a) GPR profile and b) the ERI image as shown in Figure 5 (based on an average velocity of 0.038 m ns^{-1}) and direct coring at 5

locations. Error bars in the data were calculated from the difference in peat thickness between GPR using that average velocity and ERI and that measured from the coring. Grey shading indicates estimated surface area from coring.

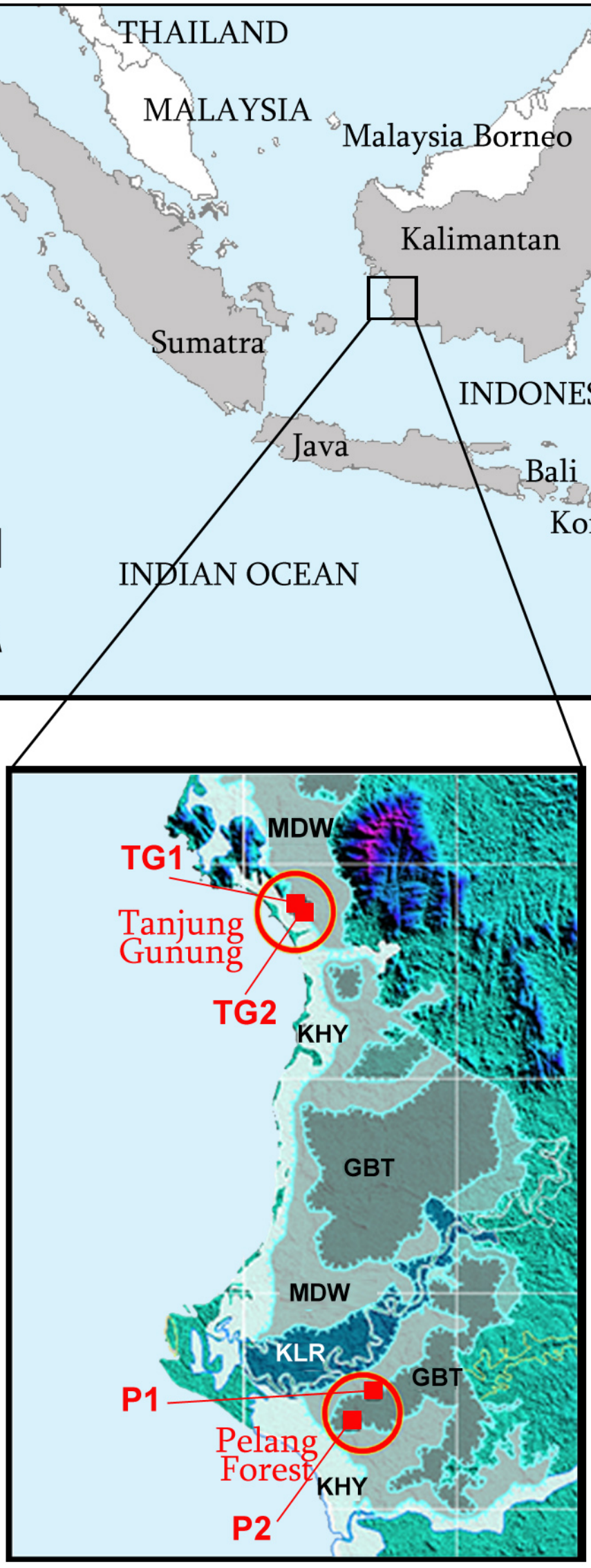

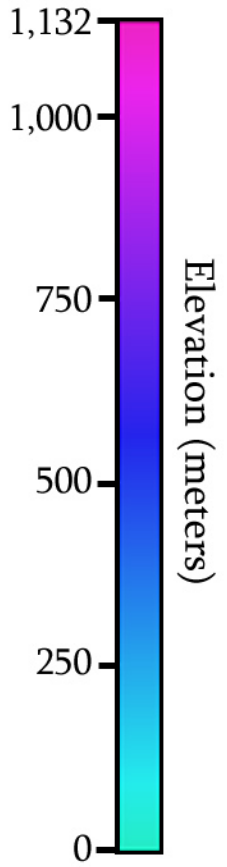

Study Sites:

TG1: Tanjung Gunung Site 1
TG2: Tanjung Gunung Site 1
P1: Pelang Forest Site 1
P2: Pelang Forest Site 2

Land system (after RePPProT):

KHY: Kahayan (alluvial plain)
GBT: Gambut (swamp)
MDW: Mendawai (swamp)
KLR: Klaru (swamp)

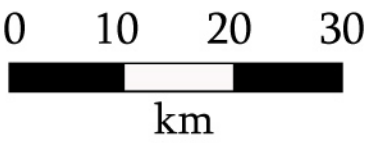

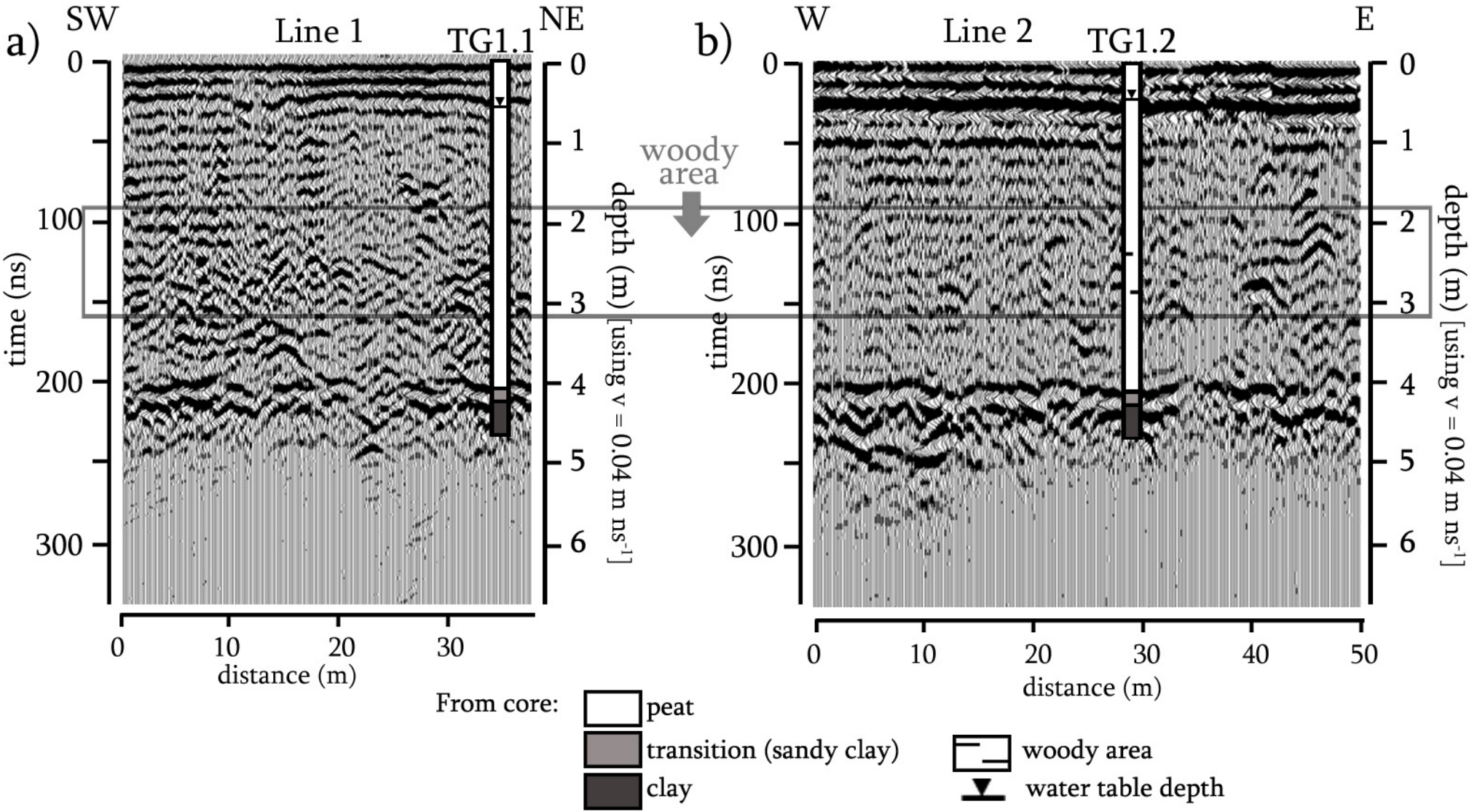
a)
SW
Line 1
TG1.1
NE
b)
W
Line 2
TG1.2
E
woody area
time (ns)
depth (m) [using v = 0.04 m ns-1]
distance (m)
From core:
peat
transition (sandy clay)
clay
woody area
water table depth

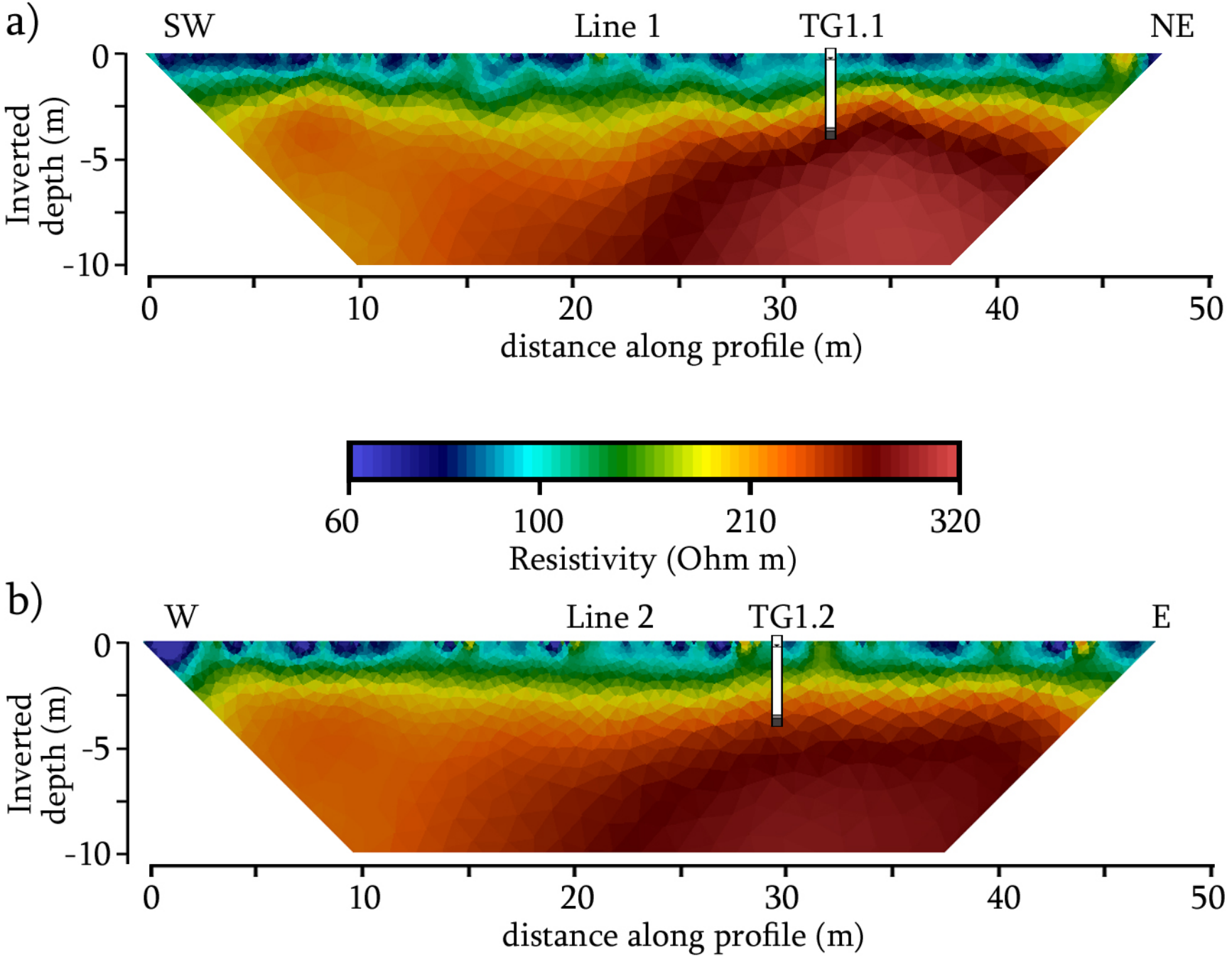
a)
SW
Line 1
TG1.1
NE
0
-5
-10
Inverted depth (m)
0
10
20
30
40
50
distance along profile (m)
60
100
210
320
Resistivity (Ohm m)
b)
W
Line 2
TG1.2
E
0
-5
-10
Inverted depth (m)
0
10
20
30
40
50
distance along profile (m)

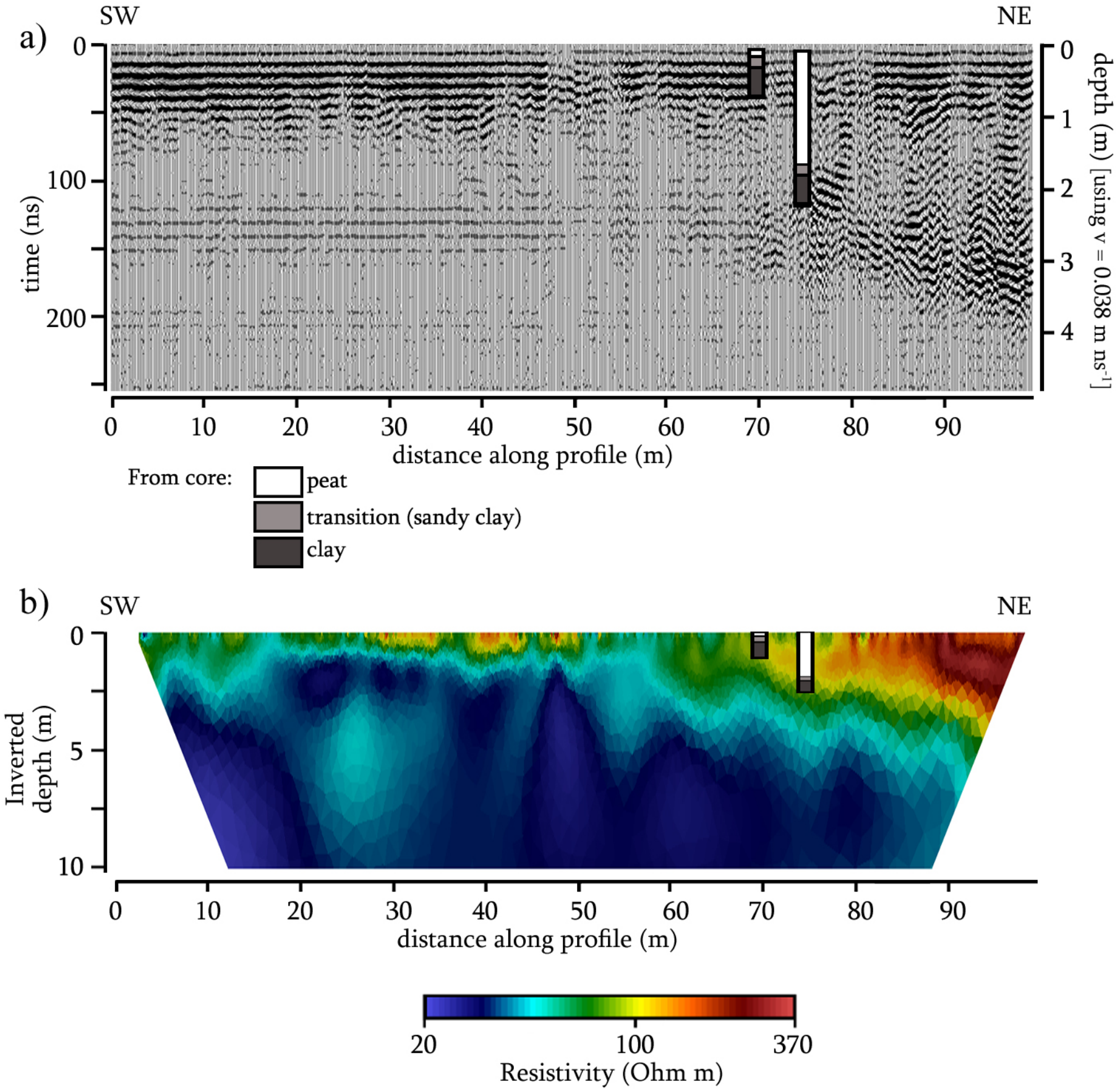
a)
SW
NE
0
100
200
time (ns)
0
1
2
3
4
depth (m) [using v = 0.038 m ns-1]
0
10
20
30
40
50
60
70
80
90
distance along profile (m)
From core:
peat
transition (sandy clay)
clay
b)
SW
NE
0
5
10
Inverted depth (m)
0
10
20
30
40
50
60
70
80
90
distance along profile (m)
20
100
370
Resistivity (Ohm m)

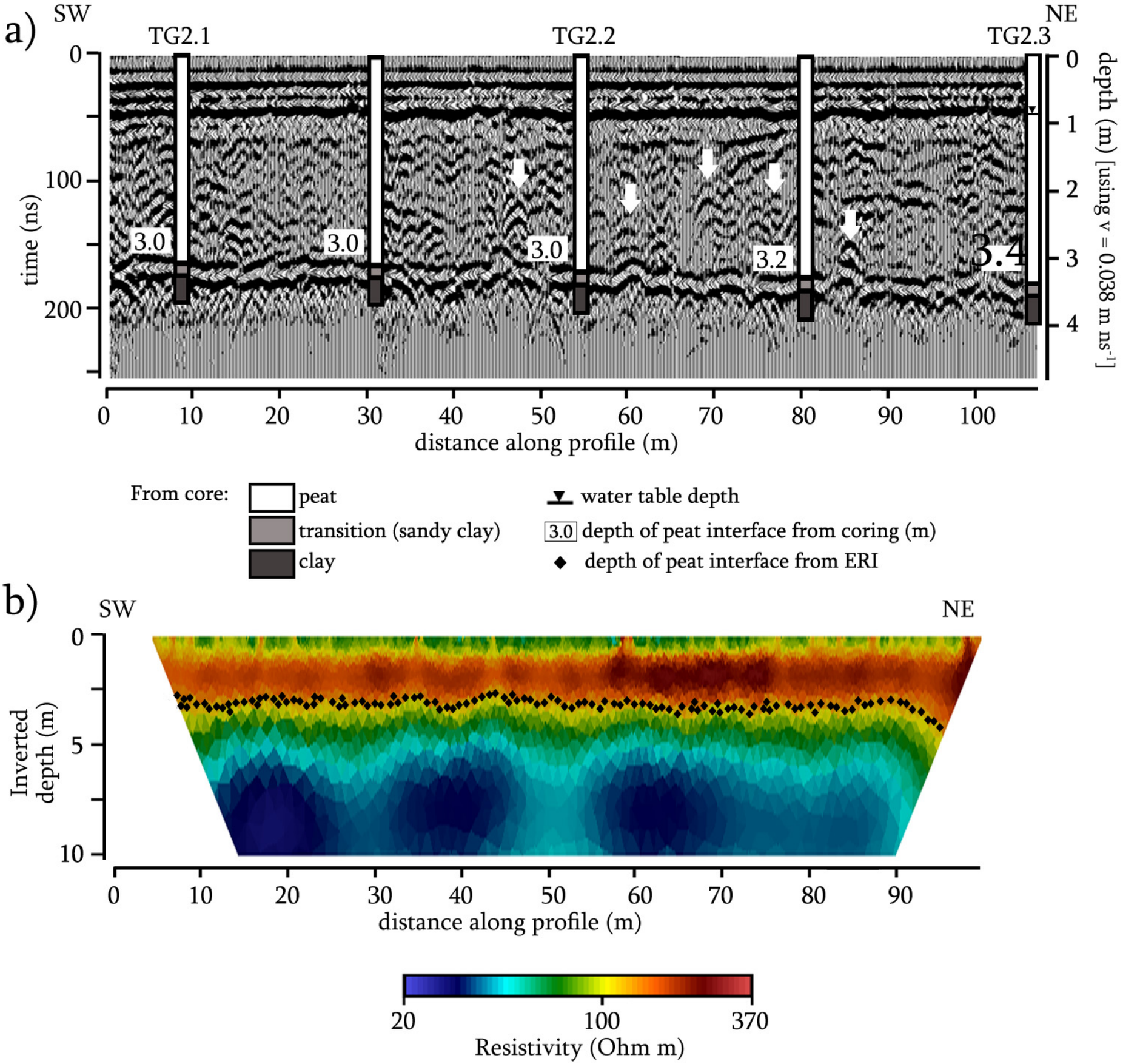
a)
SW
NE
TG2.1
TG2.2
TG2.3
time (ns)
depth (m) [using v = 0.038 m ns-1]
3.0
3.0
3.0
3.2
3.4
distance along profile (m)
From core:
peat
transition (sandy clay)
clay
water table depth
3.0 depth of peat interface from coring (m)
depth of peat interface from ERI
b)
SW
NE
Inverted depth (m)
distance along profile (m)
20
100
370
Resistivity (Ohm m)

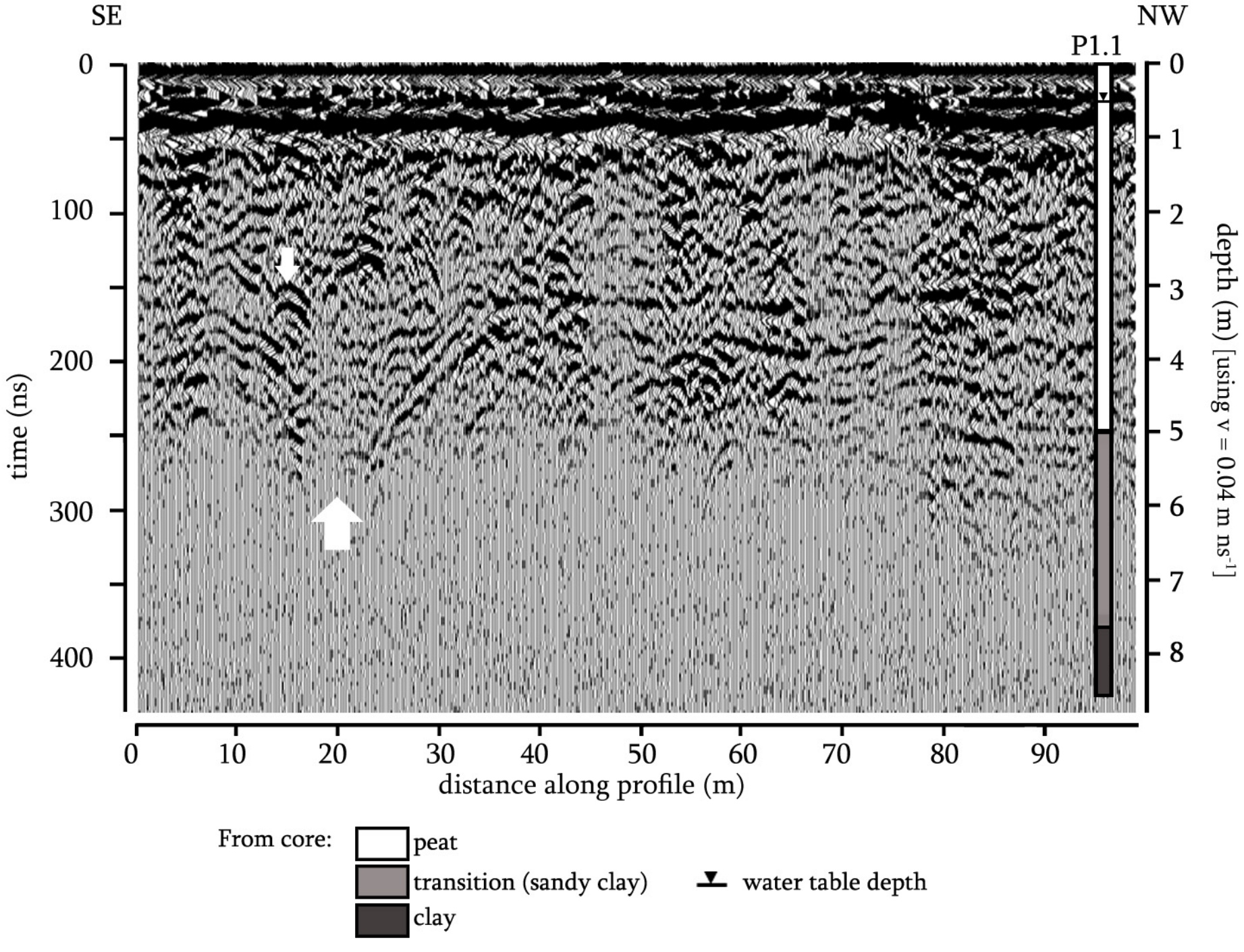
SE
NW
P1.1
0
100
200
300
400
time (ns)
0
1
2
3
4
5
6
7
8
depth (m) [using v = 0.04 m ns^{-1}]
0
10
20
30
40
50
60
70
80
90
distance along profile (m)
From core:
peat
transition (sandy clay)
clay
water table depth

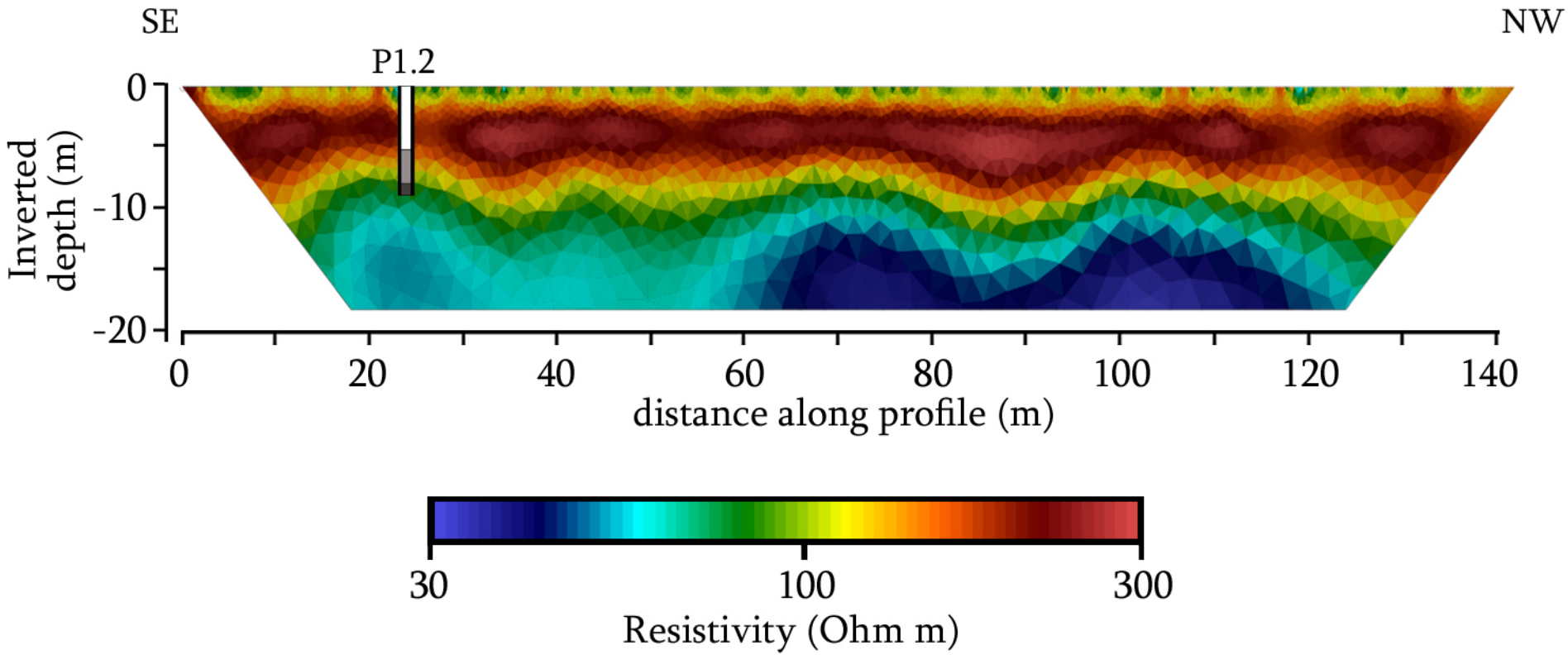
SE
NW
P1.2
0
-10
-20
Inverted depth (m)
0
20
40
60
80
100
120
140
distance along profile (m)
30
100
300
Resistivity (Ohm m)

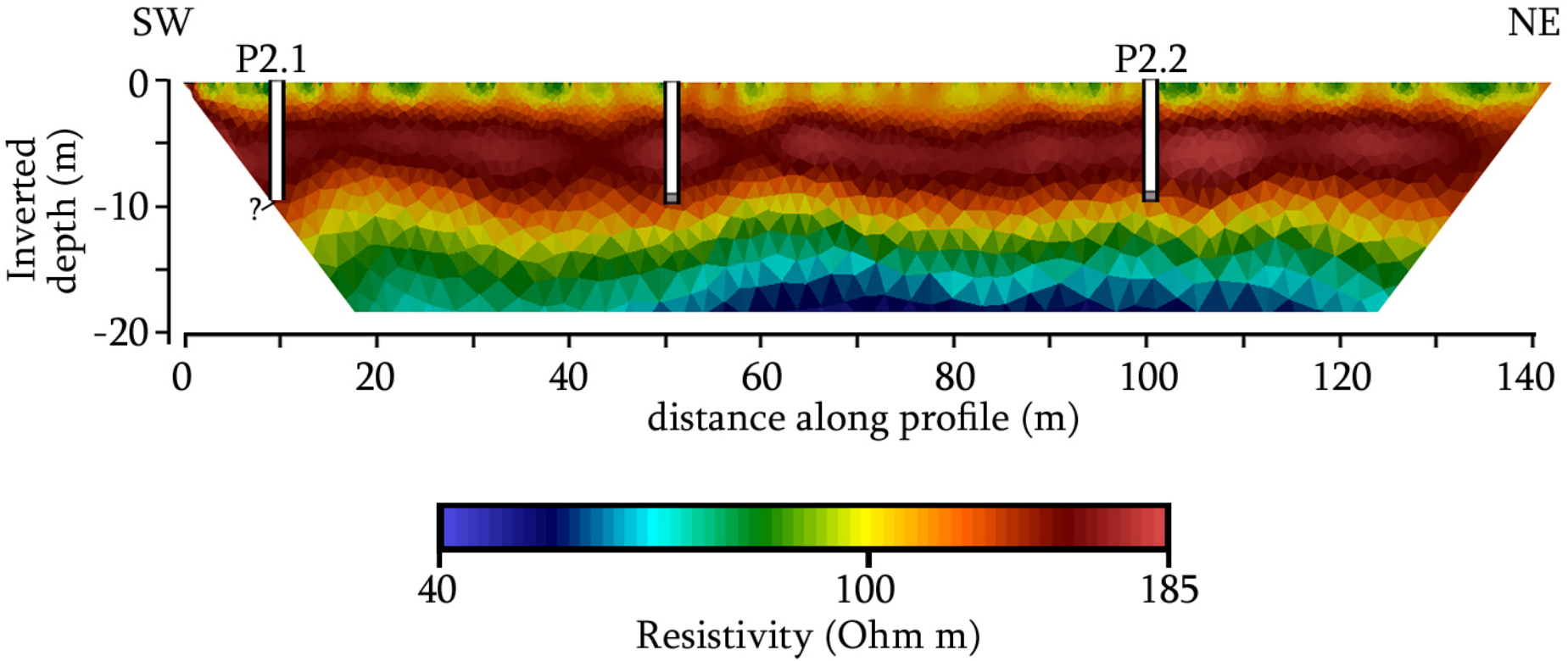
SW
NE
P2.1
P2.2
0
-10
-20
?
Inverted depth (m)
0
20
40
60
80
100
120
140
distance along profile (m)
40
100
185
Resistivity (Ohm m)

a)

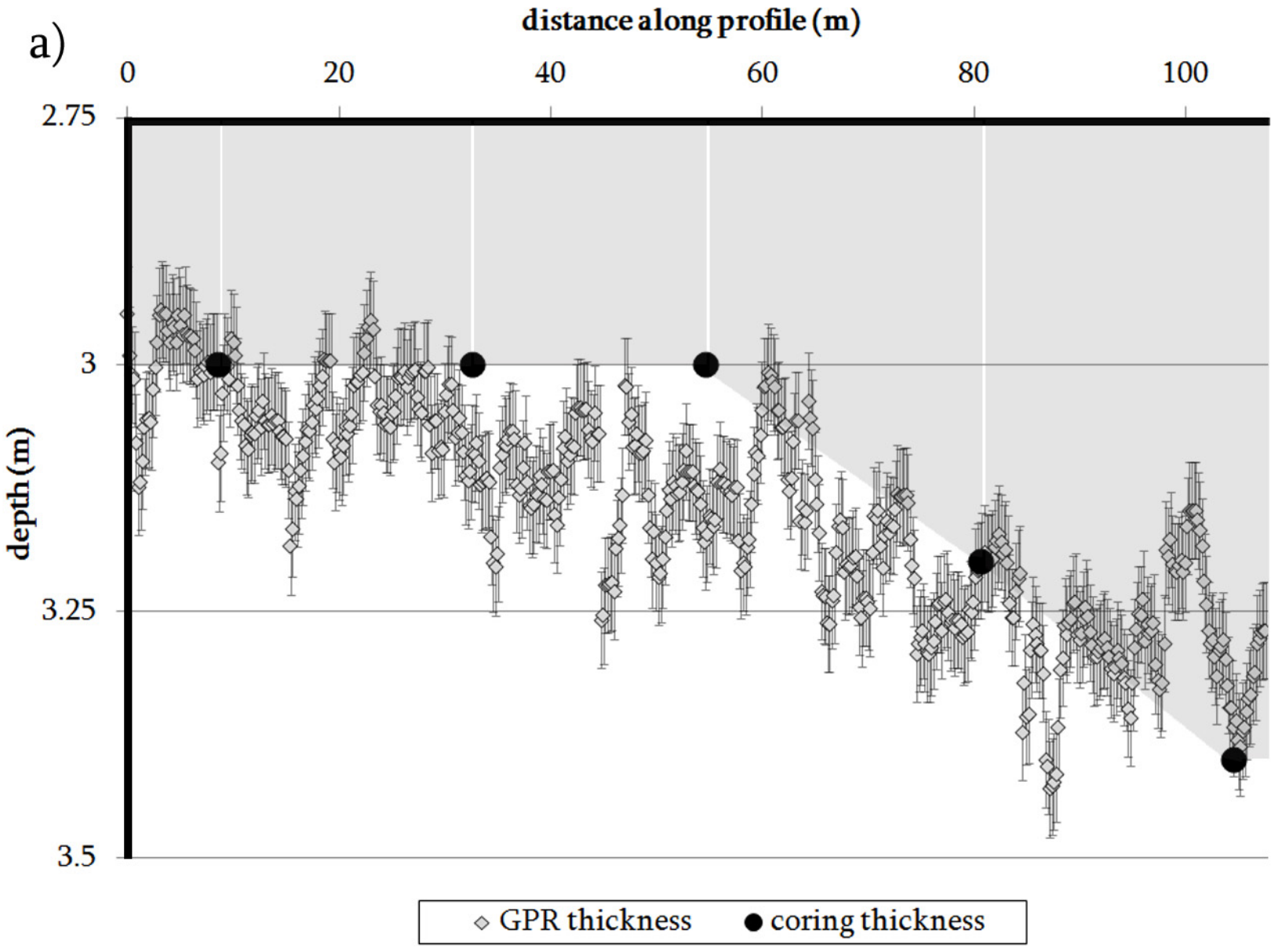
distance along profile (m)
0
20
40
60
80
100
2.75
3
3.25
3.5
depth (m)
GPR thickness
coring thickness

b)

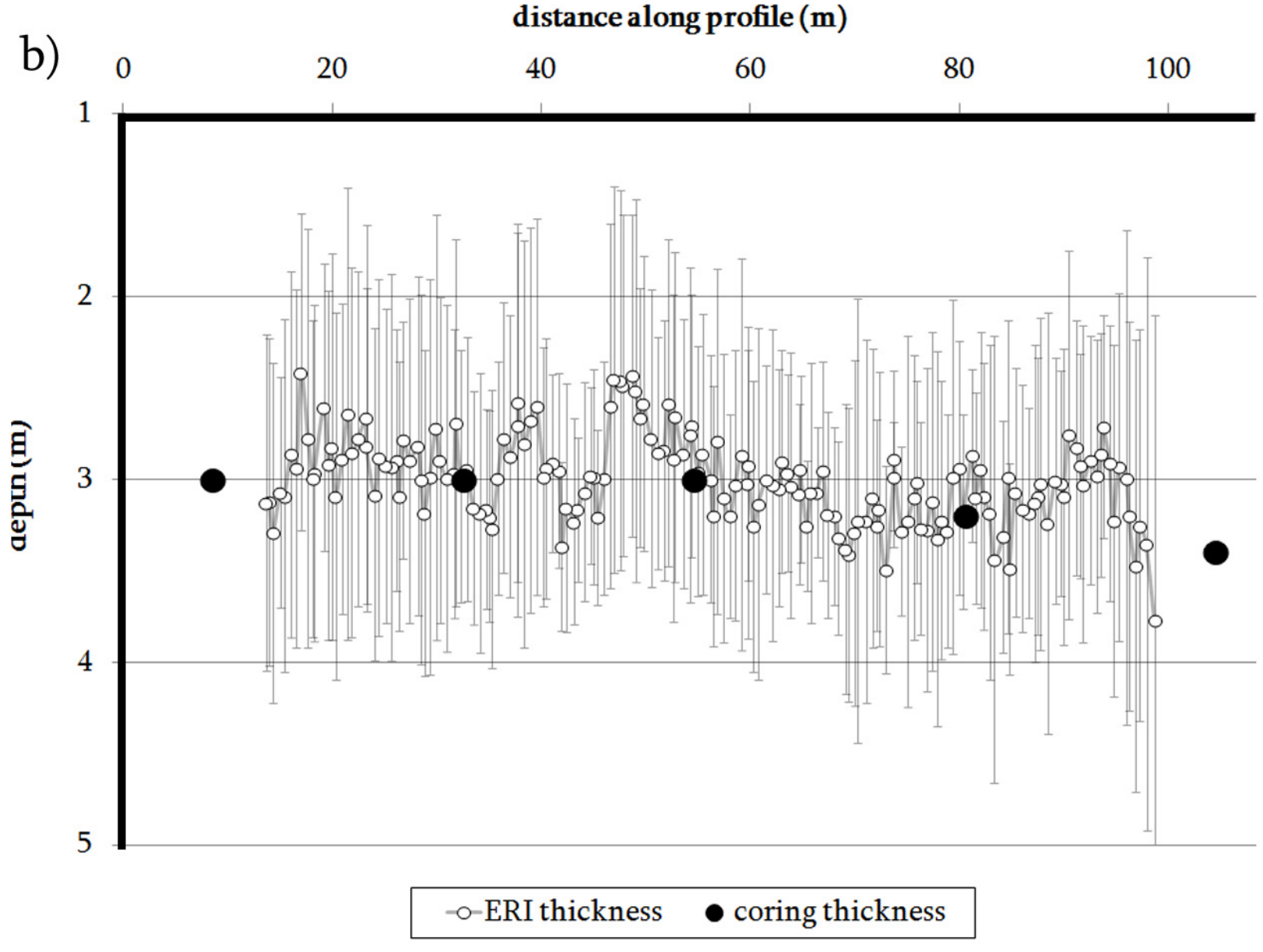
distance along profile (m)
0
20
40
60
80
100
1
2
3
4
5
depth (m)
ERI thickness
coring thickness